



2-7-2024

A novel extended reaction force/torque observer with impedance control

İlkay Turaç ÖZÇELİK
turac.ozcelik@bilgi.edu.net

Abdurrahman Eray BARAN
eray.baran@bilgi.edu.tr

Follow this and additional works at: <https://journals.tubitak.gov.tr/elektrik>





Part of the [Computer Engineering Commons](#), [Computer Sciences Commons](#), and the [Electrical and Computer Engineering Commons](#)

Recommended Citation

ÖZÇELİK, İlkay Turaç and BARAN, Abdurrahman Eray (2024) "A novel extended reaction force/torque observer with impedance control," *Turkish Journal of Electrical Engineering and Computer Sciences*: Vol. 32: No. 1, Article 13. <https://doi.org/10.55730/1300-0632.4064>
Available at: <https://journals.tubitak.gov.tr/elektrik/vol32/iss1/13>

This Article is brought to you for free and open access by TÜBİTAK Academic Journals. It has been accepted for inclusion in Turkish Journal of Electrical Engineering and Computer Sciences by an authorized editor of TÜBİTAK Academic Journals. For more information, please contact academic.publications@tubitak.gov.tr.

A novel extended reaction force/torque observer with impedance control

İlkay Turaç ÖZÇELİK^{1,*}, Abdurrahman Eray BARAN²

¹Department of Electrical and Electronics Engineering, Faculty of Engineering and Natural Sciences,
İstanbul Bilgi University, İstanbul, Türkiye

²Department of Mechatronics Engineering, Faculty of Engineering and Natural Sciences,
İstanbul Bilgi University, İstanbul, Türkiye

Received: 17.04.2023

Accepted/Published Online: 28.11.2023

Final Version: 07.02.2024

Abstract: This paper proposes a new extended version of the reaction force observer (RFOB) for high-precision motion control systems. The RFOB has been proven to be useful for many applications in the literature. However, because of the low-pass filter present inside of the RFOB, it has certain limitations. In this study, a new algorithm is proposed to compensate for filtering-based errors in the classical RFOB structure. The algorithm includes the differentiation of the observed force and scaling with a proper value. However, since the force has a noisy nature, differentiation also affects the signal's stability and performance. To resolve this issue, a new controller algorithm coupled with the proposed RFOB is formulated and implemented. The mathematical derivation of the proposed structure along with experimental validations for different force references are shown to provide a complete analysis. The results obtained from the experiments prove that the proposed observer-controller structure outperforms the existing force control architectures.

Key words: Reaction force observer, force control, impedance control, motion control, disturbance observer

1. Introduction

The adoption of high-performance force control algorithms plays a pivotal role in enabling physical interactions between machines and their surroundings. These interactions encompass a wide array of applications, including grinding processes [1], exoskeleton control [2], physical human–robot interactions [3], and collision detection [4], among others. The precise acquisition of force signals is essential for achieving stable, robust, and transparent results in these contexts. While sensor technologies offer a means to measure force signals [5], intricate electrical connections, meticulous calibration processes, and bandwidth limitations pose practical challenges.

To address these challenges, research efforts have been dedicated to devising methods for precise force signal estimation without the need for additional sensors. Estimating contact force accurately, particularly within the total reaction force, presents a formidable challenge. Noteworthy innovations include the introduction of an adaptive Kalman filter paired with a mode-switching moving average filtering technique [6]. In another domain, an optimization-based mathematical framework was proposed for precise contact force estimation in continuum robots [7]. In addition, a self-sensing structure was introduced to enhance force control in cable-tension robots, finding potential applications in surgical robot motion control [8]. Furthermore, a disturbance observer (DOB) structure, combined with torque sensors and an additional Kalman filter to mitigate noise,

*Correspondence: turac.ozcelik@bilgi.edu.net

was proven to demonstrate promising results [9]. Utilization of artificial neural networks (ANNs), and more specifically the integration of an ANN structure with a generalized momentum observer (GMO) [10], offers a solution for addressing nonlinearity and uncertainty. Additionally, the extended state observer (ESO), similar to GMO but more robust against inaccuracies in system identification [11], also showed promising results [12].

A notable method for force estimation is the use of the reaction force observer (RFOB), a disturbance observer-based technique reliant solely on the nominal model of the plant [13]. Various RFOB techniques have been developed to address specific challenges, particularly those related to bandwidth limitations and high noise levels in force control. For instance, the position-acceleration integrated disturbance observer (PAIDO) was introduced for expanding bandwidth by integrating an additional acceleration sensor [14]. This method primarily finds application in force control and is assessed using fast Fourier transform (FFT) analysis. An alternative approach involves the dither periodic component elimination (DPCE) Kalman filter, which enhances response bandwidth within the RFOB framework by effectively using periodic torque data to estimate high-order torque responses [15]. Another focus has been on addressing challenges related to reducing high-frequency noise and compensating for time-varying measurement offsets at low frequencies [16]. This was achieved by integrating force sensor measurements, motor encoder data, and motor input signals into a Kalman filter. Additionally, using Lagrangian mechanics, researchers analyzed the dynamic characteristics of the RFOB for series elastic actuators (SEAs), known as reaction force-sensing SEAs (RFSEAs) [17].

Comparative studies have indicated the promising performance of the RFOB, particularly in terms of bandwidth and application flexibility [18]. Design parameters have been found to significantly impact robust force control system stability [19]. To this end, Bode's integral theorem was used to elucidate unexpected stability issues and underscore the importance of tuning design parameters [20]. Additionally, a specific parameter calculation method tailored for the RFOB algorithm was proposed, recognizing the pivotal role of model parameters in accurate force estimation [21]. In terms of performance, the RFOB was evaluated in force sensorless workspace-based hybrid control for multiple-degrees-of-freedom robots, with a particular focus on the influence of the equivalent mass matrix configuration [22]. This analysis combined mathematical equations with experimental data.

Building on the knowledge presented, the practical applications of the RFOB have continued to evolve. In [23], the RFOB combined with an acceleration-aided Kalman filter was employed for force detection in in-circuit testing, involving the insertion of a needle-like probe into the PCB to assess electrical conductivity among the components. Furthermore, in [24], the researchers applied the RFOB and position estimation techniques to enable tactile feedback in a compact dual solenoid actuator. Additionally, the RFOB found use in ground reaction force (GRF) estimation, offering a preferred alternative to direct measurements due to load-cell limitations [25]. This facilitates the control of prostheses and legged robot models in the presence of parametric uncertainties and unmodeled dynamics through GRF estimation.

Despite its effectiveness in numerous applications, the RFOB algorithm does have limitations. The internal low-pass filter (LPF) structure restricts its suitability for high-frequency applications and impact motion profiles. In this paper, we propose an extension to the original RFOB algorithm, along with a new disturbance observer-based impedance force controller architecture, to achieve higher precision, particularly in dynamic force references and transient responses. The additional term calculated from the force estimation error through differentiation of the observer response is properly fed back to attenuate the estimation error. To mitigate the noise introduced during differentiation, a high-pass filter (HPF) is employed, which cancels out

the observed noise from the extended force estimation method. The ensuing sections of the paper include a comparison of three different force/torque estimation methods: the conventional RFOB response, the response of the proposed extended observer, and the results of the extended observer after noise cancellation with HPF. In addition to the novel estimation structure, a new disturbance observer-based impedance controller method is designed, leveraging the application of the proposed observer in the feedback loop.

The proposed observer-controller responses are compared with the classical technique in experiments using three different motion profiles: continuous interaction with a sinusoidal force reference, a sinusoidal force reference with partial impact motion, and a step force reference without impact motion. Furthermore, we conduct a time-domain and frequency-domain comparison of the dynamic behavior of the classical and the proposed structures using a sinusoidal force reference with a frequency sweep operation. The results obtained from the experiments illustrate the superior performance of the proposed observer-controller structure particularly for applications including highly dynamic motion profiles. The contributions of this study can be summarized as follows:

- A rigorous analysis of the force estimation error in the RFOB algorithm is conducted, providing insights into the limitations stemming from the internal LPF.
- An innovative extension to the RFOB algorithm is introduced, addressing LPF-induced errors by implementing differentiation and high-pass filtering for enhanced precision in dynamic force references.
- A novel force control algorithm is presented, which utilizes the proposed extended force observer structure, highlighting its potential to overcome inherent limitations and enhance accuracy.
- Comprehensive experiments are conducted to validate the increased bandwidth capabilities of the proposed approach, particularly in handling dynamic force references, thus demonstrating its practical advantages.

The organization of the paper is as follows: In Section 2, the classical reaction force observer structure is explained. Section 3 is reserved for the derivation of the proposed extended RFOB algorithm. In Section 4, the traditional and the proposed force control architectures are formulated. The real-time experimental results are presented and discussed in Section 5. Finally, in Section 6, concluding remarks are given.

2. Derivation of the classical reaction force observer

In this section, the classical method for the RFOB is derived as explained in [13] and [26]. Without loss of generality, the model of a motion control system with a single degree of freedom (DOF) can be given as follows:

$$M(x)\ddot{x}(t) + b(x, \dot{x}) + g(x) + \tau^{ext}(t) = \tau(t). \quad (1)$$

In Eq. (1), $x, \dot{x}, \ddot{x} \in \mathbb{R}^{1 \times 1}$, all functions of time, represent the position, velocity, and acceleration responses of the system, respectively. $M(x) \in \mathbb{R}^{1 \times 1}$ is the inertia, $\tau^{ext}(t) \in \mathbb{R}^{1 \times 1}$ is the total external torque that acts on the system, and $\tau(t) \in \mathbb{R}^{1 \times 1}$ is the input torque. Here, $b(x, \dot{x}) \in \mathbb{R}^{1 \times 1}$ stands for the dynamic forces, which include Coriolis, viscous friction, and centripetal forces, while the term $g(x) \in \mathbb{R}^{1 \times 1}$ represents the forces due to gravitation. The input torque can be formulated as $\tau(t) = K_t i(t)$, where K_t is the torque constant and $i(t) \in \mathbb{R}^{1 \times 1}$ is the current supplied to the system. Under the assumption that small variations of the nominal parameters are compensated with a disturbance observer [27], one can write Eq. (1) as follows:

$$M_n(x)\ddot{x}(t) + b(x, \dot{x}) + g(x) + \tau^{ext}(t) = K_n i(t). \quad (2)$$

involving high-frequency operations and motion profiles characterized by impacts. Hence, in this section, we put forth an extension to the original RFOB algorithm. The derivation is made on the basis of an error analysis for the classical RFOB method. The force estimation error for the classical RFOB structure can be given as follows:

$$\Delta T(s) = T^{ext}(s) - \hat{T}^{ext}(s). \quad (7)$$

As also mentioned in the previous section, the estimated external torque is the low-pass filtered version of the applied external torque. Hence, one can reformulate Eq. (7) as follows:

$$\Delta T(s) = T^{ext}(s) - T^{ext}(s) \frac{g_l}{s + g_l}. \quad (8)$$

Eq. (8) can be rearranged to yield the following expression:

$$\Delta T(s) = T^{ext}(s) \left(1 - \frac{g_l}{s + g_l}\right) = T^{ext}(s) \frac{s}{s + g_l}. \quad (9)$$

The interpretation of the identity obtained in Eq. (9) is straightforward. The high-frequency component of the reaction force signal, beyond the cut-off frequency of the internal LPF, constitutes the main error in reaction force estimation. In order to achieve a more simplified form, Eq. (9) can be rearranged as follows:

$$\Delta T(s) = T^{ext}(s) \frac{g_l}{s + g_l} \frac{s}{g_l} = \hat{T}^{ext}(s) \frac{s}{g_l}. \quad (10)$$

The expression given in Eq. (10) opens the door for a better interpretation of the force estimation error. Using the classical RFOB structure, the error in reaction force estimation is simply equal to the scaled derivative of the estimated force signal. Furthermore, looking at Eq. (10), it is clear that the classical method produces better results with higher cut-off frequencies for observing reaction forces. However, there is a trade-off between system response and noise due to the effect of the LPF. Selection of a high g_l value results in smaller estimation error in exchange for increasing noise amplitude. This relationship results in a degraded estimation performance specifically for dynamic force signals such as impact forces.

Originating from Eq. (10), the proposed method introduces error feedback into the system. This allows the observed force signal to have a wider bandwidth. Although this improves the system's performance, it may not be practical for real-time applications due to the amplification of the inherent noise in the force signal during differentiation. To address this issue, a new HPF is introduced that can effectively filter out noise when the cut-off frequency is selected appropriately. Accordingly, the estimated torque of the proposed structure can be expressed as follows:

$$\hat{T}^{ext}(s) = T^{ext}(s) \frac{g_l}{s + g_l} + T^{ext}(s) \frac{s}{s + g_l} - T^{ext}(s) \frac{s}{s + g_h}. \quad (11)$$

In Eq. (11), g_l stands for the LPF cut-off frequency and g_h represents the HPF cut-off frequency.

Eq. (11) indicates that the response torque estimation leads to identical outcomes for the classical and proposed structures if the respective cut-off frequencies of the LPF and HPF are the same. However, if these two frequencies are selected differently, the new observer structure may provide a wider bandwidth for the estimated force, which is particularly important in cases where the interaction force changes rapidly. The first LPF of Eq. (11) provides the same estimation as that of the classical RFOB module, which has an estimation

error as shown in Eq. (10). The first HPF in Eq. (11) is there to compensate for this error of the classical RFOB structure. However, the introduction of this HPF also contributes negatively to the high-frequency noise component of the estimated signal. Therefore, the last HPF of Eq. (11) is introduced, which cancels out the noise component beyond the cut-off frequency of g_h . To illustrate the performance of the proposed structure, a new force tracking error is formulated in the following section and a new impedance controller algorithm is proposed accordingly. The proposed force estimation structure's block diagram is shown in Figure 2. Further details regarding the torques presented in Figure 2, denoted as $\hat{T}^c(s)$, $\hat{T}^e(s)$, $\hat{T}_{env}^{res}(s)$, and $\hat{T}^n(s)$, are provided in Section 4.2.

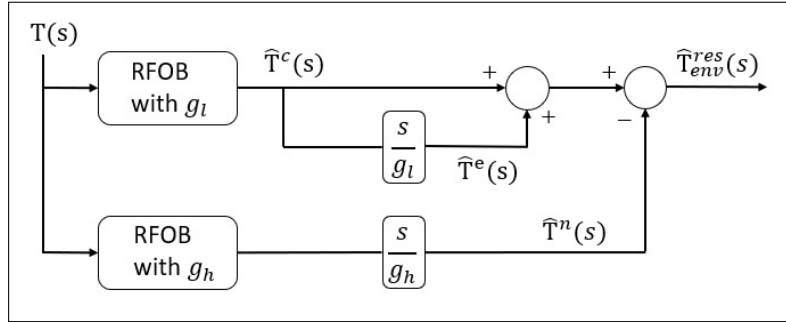


Figure 2. Block diagram of the proposed reaction force observer.

4. Controller derivation

This section is dedicated to the formulation of acceleration-based impedance force control architectures. For the sake of a complete analysis, first, the classical impedance force control architecture with a disturbance observer will be derived. After that, the proposed force controller scheme will be presented. The proposed RFOB structure will be used as the fundamental tool for the derivation of the new controller. For modeling purposes, the reaction of the environment is assumed to be overruled by a spring [29], which has the following force relationship:

$$\tau^{res}(t) = K_e x^{res}(t). \quad (12)$$

Eq. (12) represents the dominant reaction force from the environment and K_e signifies the spring constant.

4.1. Classical force controller

In order to derive the controller structure, one can define the force tracking error as follows:

$$\varepsilon(t) = \tau^{ref}(t) - \hat{\tau}^{res}(t). \quad (13)$$

Since the disturbances in the system are assumed to be compensated via a disturbance observer, the main objective of the outer loop controller should be formulating the desired accelerations that will enforce the convergence of the error in Eq. (13) to zero as shown in [30]. Given that the environmental force only depends on the position response, the desired acceleration can be obtained by substituting Eq. (13) into the following second-order differential equation:

$$\ddot{\varepsilon}(t) + \alpha \dot{\varepsilon}(t) + \beta \varepsilon(t) = 0. \quad (14)$$

Convergence to zero can be guaranteed by picking strictly positive controller gains (i.e. $\alpha, \beta \in \mathbb{R} > 0$). Expanding Eq. (14) using the content of error from Eq. (13) results in the following expression:

$$\ddot{\tau}^{ref}(t) - \ddot{\hat{\tau}}^{res}(t) + \alpha(\dot{\tau}^{ref}(t) - \dot{\hat{\tau}}^{res}(t)) + \beta(\tau^{ref}(t) - \hat{\tau}^{res}(t)) = 0. \quad (15)$$

Furthermore, the environment model assumed in Eq. (12) can also be appropriately substituted in Eq. (15), which results in the following equality:

$$\ddot{\tau}^{ref}(t) - K_e \ddot{x}^{res}(t) + \alpha(\dot{\tau}^{ref}(t) - K_e \dot{x}^{res}(t)) + \beta(\tau^{ref}(t) - \hat{\tau}^{res}(t)) = 0. \quad (16)$$

Enforcement of the dynamics given in Eq. (16) provides the tracking of the reference torque by the system. In order to achieve this goal, one can single out the response acceleration and supply it as the desired acceleration as follows:

$$\ddot{x}^{res}(t) = \ddot{x}^{des}(t) = \frac{1}{K_e} [\ddot{\tau}^{ref}(t) + \alpha(\dot{\tau}^{ref}(t) - K_e \dot{x}^{res}(t)) + \beta(\tau^{ref}(t) - \hat{\tau}^{res}(t))]. \quad (17)$$

In Eq. (17), $\ddot{x}^{res}(t)$ and $\ddot{x}^{des}(t)$ stand for the response and desired accelerations, respectively. For a comprehensive representation of the classical force control architecture, a block diagram is provided in Figure 3.

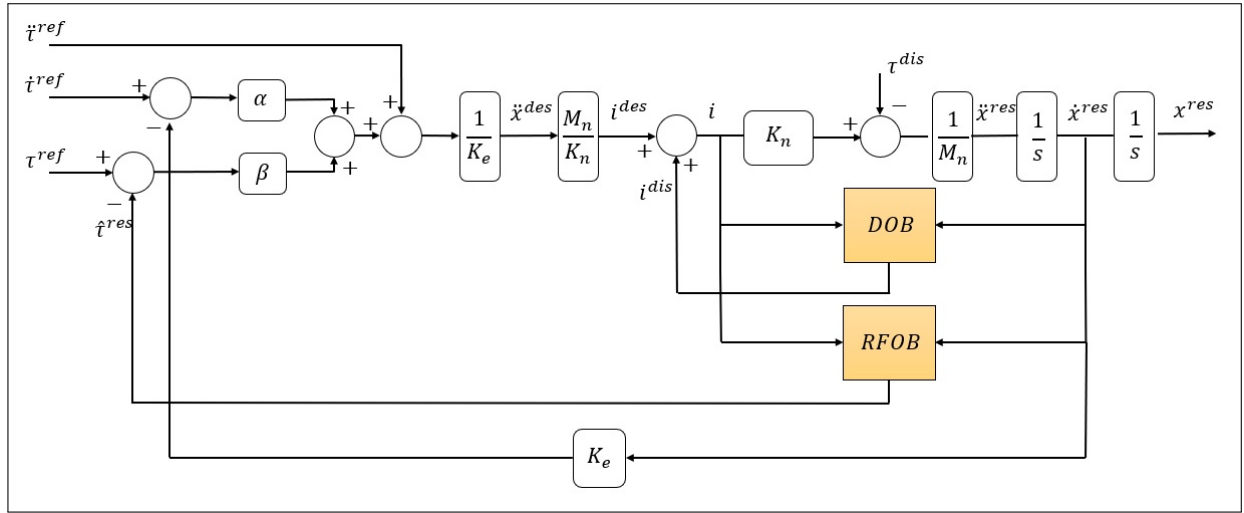


Figure 3. Block diagram of the classical force controller scheme.

4.2. Proposed force controller

In this section, a novel force control architecture is formulated, which utilizes the proposed extended RFOB structure. In contrast to the traditional framework, the proposed force controller makes use of three distinct reaction force components as detailed in Eq. (11). The mathematical expressions for these force components can be given as follows:

$$\hat{T}^c(s) = T^{ext}(s) \left(\frac{g_l}{s + g_l} \right), \quad (18)$$

$$\hat{T}^e(s) = T^{ext}(s) \left(\frac{g_l}{s + g_l} \right) \frac{s}{g_l}, \quad (19)$$

$$\hat{T}^n(s) = \mathbf{T}^{ext}(s) \left(\frac{g_h}{s + g_h} \right) \frac{s}{g_h}. \quad (20)$$

The equations given above are all representations provided in the Laplace domain. Leveraging the insights derived from Eq. (4), it becomes possible to express these torques in the time domain as follows:

$$\hat{\tau}^c(t) = \hat{\tau}^{res}(t), \quad (21)$$

$$\hat{\tau}^e(t) = \dot{\hat{\tau}}^{res}(t) \frac{1}{g_l}, \quad (22)$$

$$\hat{\tau}^n(t) = \dot{\hat{\tau}}^{res}(t) \frac{1}{g_h}. \quad (23)$$

Here, $\hat{\tau}^c(t)$, $\hat{\tau}^e(t)$, $\hat{\tau}^n(t)$, and $\hat{\tau}^{res}(t)$ denote the classical torque estimation, the extended torque estimation, the high-frequency noise over the estimated torque, and the classical RFOB-based estimated torque response, respectively. It is important to understand that the estimated reaction torques obtained from Eqs. (18) and (20) will be different due to their distinct LPF cut-off frequencies. However, both estimates correspond to the same estimated torque resulting from the system's interaction with the environment. This is because the two RFOBs – one with a LPF and the other with a HPF – produce outputs that capture different components of the force signal. Hence, without loss of generality, one can express the environment's force response as follows:

$$\hat{\tau}_{env}^{res}(t) = \hat{\tau}^{res}(t) + \dot{\hat{\tau}}^{res}(t) \frac{1}{g_l} - \dot{\hat{\tau}}^{res}(t) \frac{1}{g_h}. \quad (24)$$

Here, $\hat{\tau}_{env}^{res}(t)$ stands for the total response torque captured from environment. Similar to the previous section, one can write the force tracking error for the controller as follows:

$$\epsilon(t) = \tau^{ref}(t) - \hat{\tau}_{env}^{res}(t). \quad (25)$$

At this point, the identity presented in Eq. (24) can be inserted into Eq. (25), taking into account the assumption of a model dominated by spring characteristics. This modification leads to a redefinition of the tracking error as follows:

$$\epsilon(t) = \tau^{ref}(t) - K_e x^{res}(t) - K_e \dot{x}^{res}(t) \frac{1}{g_l} + K_e \dot{x}^{res}(t) \frac{1}{g_h}. \quad (26)$$

Since Eq. (26) contains the velocity response, in order to attain the desired acceleration for the control, a first-order differential equation can be used yielding the following expressions:

$$\dot{\epsilon}(t) + C\epsilon(t) = 0, \quad (27)$$

$$\dot{\tau}^{ref}(t) - K_e \dot{x}^{res}(t) - \frac{K_e}{g_l} \ddot{x}^{res}(t) + \frac{K_e}{g_h} \ddot{x}^{res}(t) + C(\tau^{ref}(t) - \hat{\tau}_{env}^{res}(t)) = 0. \quad (28)$$

Here, $C > 0$ is the gain of the controller, standing for the exponential convergence rate of the force tracking error to zero. Similar to Eq. (17), under the assumption that the system's disturbances are mitigated through a DOB, the desired acceleration will be facilitated from the response acceleration as follows:

$$\ddot{x}^{des}(t) = \ddot{x}^{res}(t) = \frac{g_l g_h}{K_e (g_h - g_l)} [\dot{\tau}^{ref}(t) - K_e \dot{x}^{res}(t) + C(\tau^{ref}(t) - \hat{\tau}_{env}^{res}(t))]. \quad (29)$$

The tracking of the desired acceleration given in Eq. (29) enforces the naturally stable dynamics given in Eq. (27), providing exponential convergence of the tracking error to zero. The proposed controller benefits from the distinct cut-off frequencies of the filters, which highlights the importance of carefully selecting them. The cut-off frequency not only filters out the noise but also has a significant impact on improving the controller's performance. Furthermore, one should notice that g_h must be larger than g_l to obtain a properly functioning controller. For the sake of a complete analysis, a depiction of the proposed force controller is given in Figure 4.

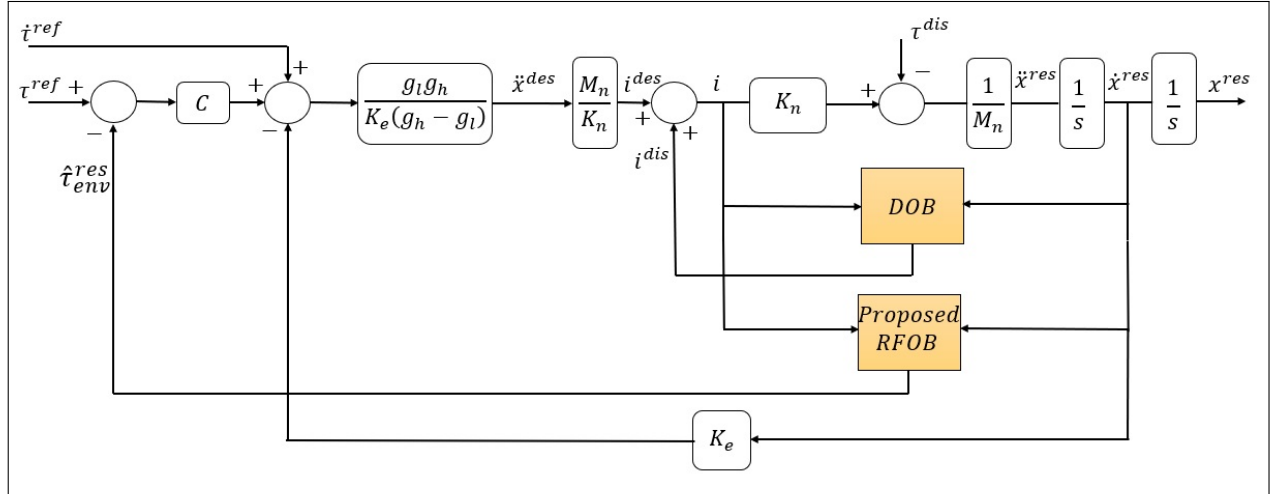


Figure 4. Block diagram of the proposed force controller scheme.

5. Results

This section is dedicated to presenting the experimental results. It is important to note here that the classical and the proposed controllers have different numbers of gains to adjust. Hence, the parameter selection process will be explained first. Next, a brief description of the experimental platform will be provided. The results of two sets of experiments, each with different reference profiles, will then be presented. Finally, the results of a sinusoidal frequency sweep experiment will be displayed along with a comparison of the frequency-domain responses for these two controllers.

5.1. Controller gains

It is observable from Eqs. (17) and (29) that the classical and proposed controllers have differing numbers of gains. To present a comprehensive comparison between the two controller structures, the controller gains for the experimental validation were selected as follows:

$$s^2 + \alpha s + \beta = (s + C)^2. \quad (30)$$

The identity given in Eq. (30) ensures that the two controllers have the same exponentially converging error rate. Hence, this selection provides an opportunity to compare the performances of the proposed and classical control architectures regardless of the effects of the selected controller gains.

5.2. Experimental platform

For the experimental validation, one Faulhaber LM2070 series linear motor is used. The motor contains an encoder with $0.5 \mu\text{m}$ resolution. The implementation of the controller in a real-time environment is done with a B&R 1586 PLC while the execution is performed with a C code running at 5 kHz loop frequency. To better observe the performance of the two control structures, the interacted environment is selected to have relatively high stiffness, which is more difficult to control due to unintended oscillations in the first contact. A depiction of the platform used in the experiments is given in Figure 5.

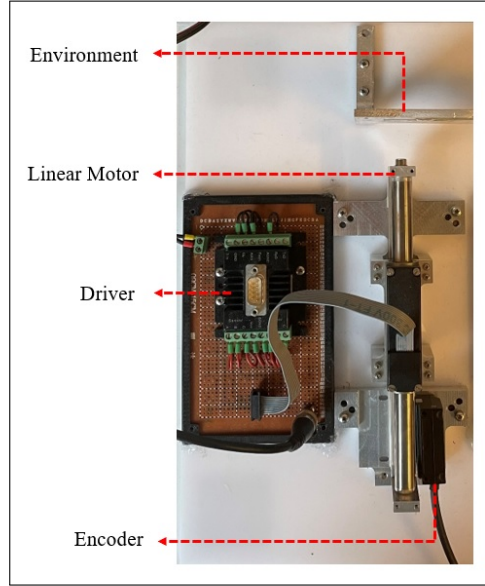


Figure 5. Experimental setup.

5.3. Experiments

The experiments involve a comparison between the classical and proposed controllers. For this purpose, three types of force references are used, namely a sinusoidal force with continuous interaction, a sinusoidal force reference with impact motion, and step force references. The equations for these references are listed in Table 1. To better compare the responses of the two control architectures, the first experiment set (i.e. experiment

Table 1. References for experiment sets 1 and 2.

Constant Force	$8 + 2\cos(2\pi f) \text{ N}$
Impact Force	$3 + 10\cos(2\pi f) \text{ N}$
Step Force	12 N

set 1) is carried out with the same controller gains as explained in Eq. (30). On the other hand, a secondary comparison of the controllers is provided in the second experiment set (i.e. experiment set 2) by independently adjusting the controller gains to give their respective best performances. The results obtained from these two experiment sets are given in Figure 6 and Figure 7, respectively. Furthermore, to see the bandwidth of the controller, a frequency sweep experiment is designed where the reference force signal frequency is continuously changed from 0 to 13 Hz in 6 s with the following reference force signal:

$$y(t) = 8 + 6\cos\left(\frac{2\pi f}{6}t^2\right). \quad (31)$$

The controller gains for the sweeping experiment (i.e. experiment set 3) are selected to be the same as in experiment set 1. The time-domain response and the frequency response of experiment set 3 are shown in Figures 8A and 8B, respectively. For all three experiment sets, the stiffness of the environment is selected as 85,000 N/m in the controllers, the cut-off frequency of the velocity observer is set to 2500 rad/s, and the cut-off frequency of the disturbance observer is set to 1500 rad/s. The parameters of the controllers used in the experiments are listed in Table 2.

Table 2. Parameters used in the experiments.

	Exp. Set-1 both methods	Exp. Set-2 proposed method	Exp. Set-2 classical method
C	220	180	-
α	440	-	210
β	48,400	-	85,000
g_l	700	700	2500
g_h	900	900	-

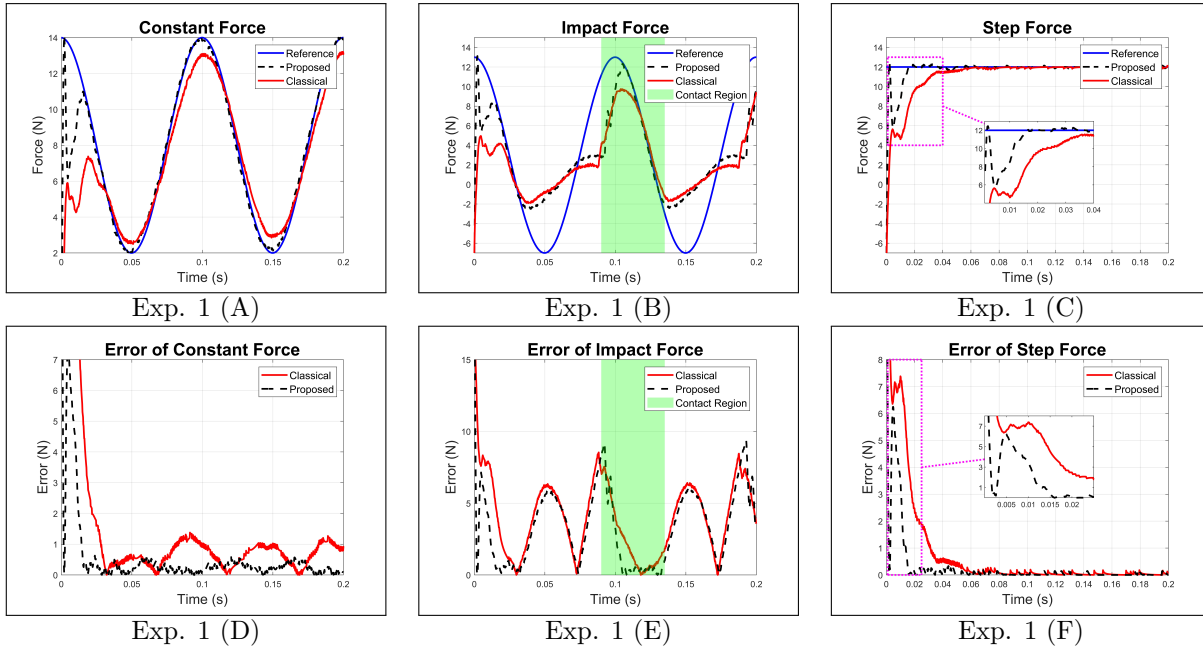


Figure 6. Results of experiment set 1: sinusoidal force (A), impact force (B), step force (C), constant force error (D), impact force error (E), and step force error (F).

The experimental results presented in Figure 6 and Figure 7 clearly demonstrate that the proposed controller outperforms the classical method in terms of both transient and steady-state responses. The proposed controller achieves better tracking of the desired forces for three different types of reference inputs considered in experiment set 1, namely the sinusoidal force reference with continuous contact, sinusoidal force reference with contact loss (i.e. impact motion), and step force reference with continuous contact, respectively.

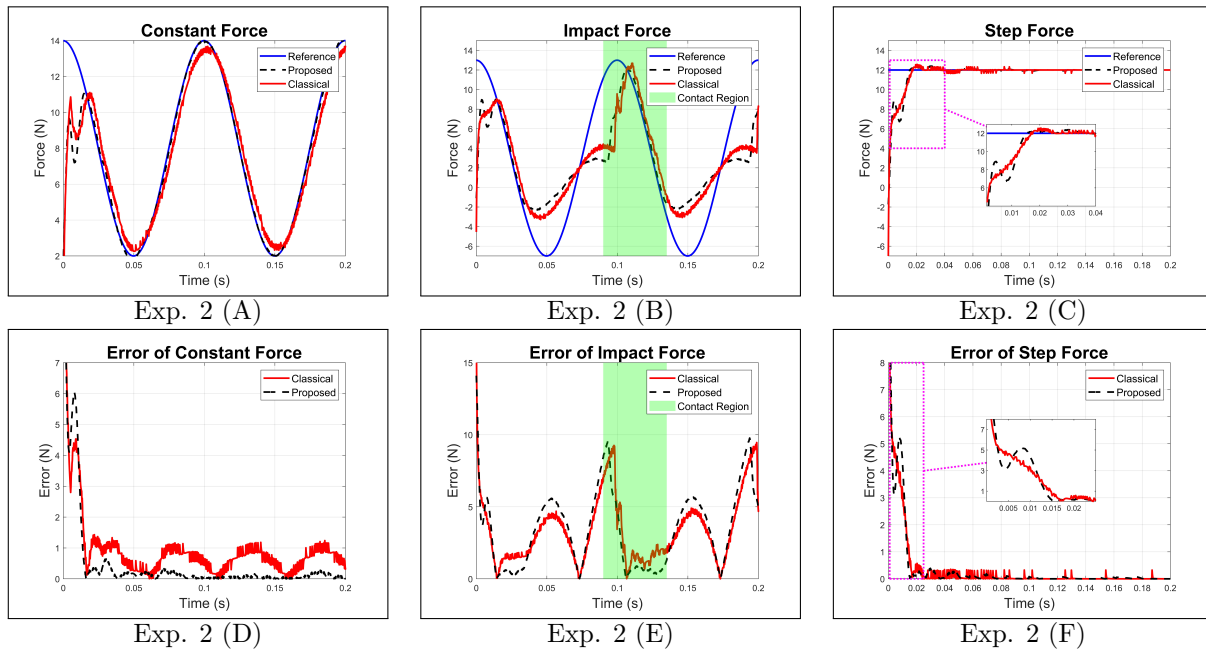


Figure 7. Results of experiment set 2: constant force (A), impact force (B), step force (C), constant force error (D), impact force error (E), and step force error (F).

It is evident from the results that the proposed technique exhibits better performance in terms of the tracking accuracy and phase delay compared to the classical method. This means that the proposed controller can respond more quickly to the changes in the system, which can lead to an improved control performance and stability. Further investigation using Bode plots, as shown in Figure 8B, confirmed that the magnitude response of the proposed method converges to zero more quickly and is closer to zero in the steady state. This makes the proposed estimation and control scheme a much better option for scenarios where the reference force signal has a highly dynamic structure, as in the case of a hard contact force control example.

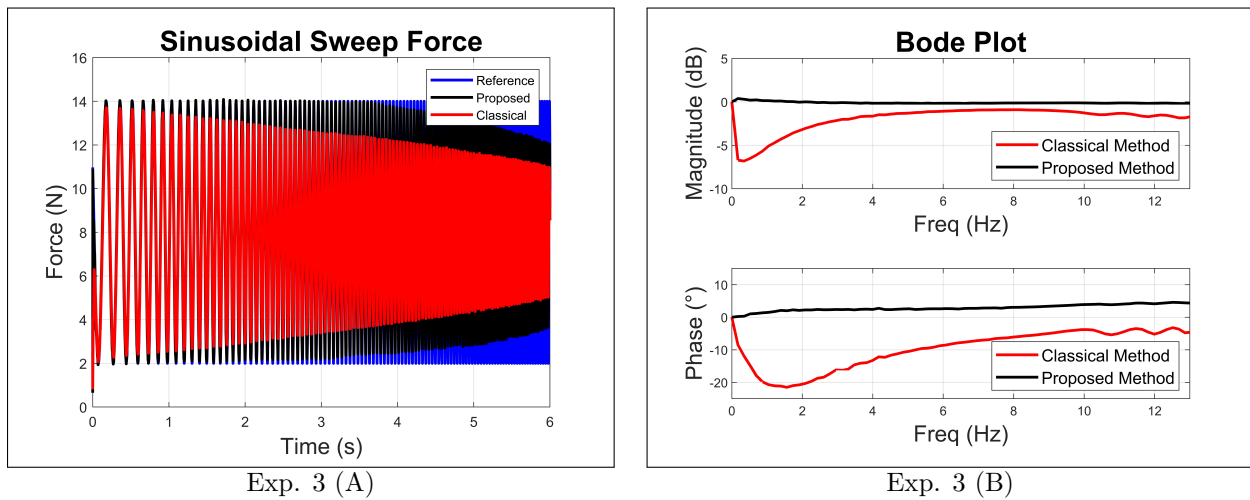


Figure 8. Results of experiment set 3: sinusoidal sweep (A) and Bode plots (B).

For better comparison of the results, numerical evaluations are made where root-mean square (RMS) errors are calculated for both experiment sets. The RMS error results are listed in Table 3 and Table 4. In both sets of experiments, the proposed extended RFOB structure consistently outperforms the classical one across all three force references. Additionally, it is evident that the second set of experiments yields lower error rates. In conclusion, the error results align with the preceding discussion of the figures' outcomes.

Table 3. RMS error results for experiment set 1.

	Constant force	Impact force	Step force
Classical method	0.63	2.4	0.04
Proposed method	0.24	1.8	0.02

Table 4. RMS error results for experiment set 2.

	Constant Force	Impact Force	Step Force
Classical Method	0.59	3.2	0.015
Proposed Method	0.09	2.3	0.012

6. Conclusion

In this study, a novel algorithm has been presented to address the filtering-related inaccuracies within the conventional RFOB design. This algorithm involves computing the derivative of the observed force and adjusting it with an appropriate factor. However, given the inherently noisy nature of force data, differentiation can also impact the signal's stability and performance. To tackle this challenge, a new controller algorithm has been developed and integrated with the proposed RFOB. This study has detailed the mathematical derivation of this enhanced structure and offered experimental validations with diverse force references to furnish a comprehensive analysis. The experimental results clearly demonstrate the superior performance of the proposed observer-controller configuration compared to existing force control systems. The proposed observer-controller setup is anticipated to be valuable, especially for systems that demonstrate extremely dynamic force reactions, such as legged locomotion applications, haptic feedback devices, medical robotic devices, and teleoperation systems. Future research endeavors aimed at enhancing the proposed structure could explore the implementation of more specialized filters, such as second-order filters. Furthermore, the utilization of a Kalman filter to mitigate the high-frequency noise in the proposed configuration would also present opportunities for innovative approaches.

Acknowledgment

This study was partially supported by Internal Research Grant RDI.2020.1 from İstanbul Bilgi University.

References

- [1] Wang Q, Wang W, Zheng L, Yun C. Force control-based vibration suppression in robotic grinding of large thin-wall shells. *Robotics and Computer-Integrated Manufacturing* 2021; 67: 102031. <https://doi.org/10.1016/j.rcim.2020.102031>
- [2] Gui K, Liu H, Zhang D. A practical and adaptive method to achieve EMG-based torque estimation for a robotic exoskeleton. *IEEE/ASME Transactions on Mechatronics* 2019; 24 (2): 483-494. <https://doi.org/10.1109/TMECH.2019.2893055>

- [3] He W, Xue C, Yu X, Li Z, Yang C. Admittance-based controller design for physical human–robot interaction in the constrained task space. *IEEE Transactions on Automation Science and Engineering* 2020; 17 (4): 1937-1949. <https://doi.org/10.1109/TASE.2020.2983225>
- [4] Birjandi SAB, Haddadin S. Model-adaptive high-speed collision detection for serial-chain robot manipulators. *IEEE Robotics and Automation Letters* 2020; 5 (4): 6544-6551. <https://doi.org/10.1109/LRA.2020.3015187>
- [5] Liu Y, Bao R, Tao J, Li J, Dong M et al. Recent progress in tactile sensors and their applications in intelligent systems. *Science Bulletin* 2020; 65 (1): 70-88. <https://doi.org/10.1016/j.scib.2019.10.021>
- [6] Cao F, Docherty PD, Ni S, Chen XQ. Contact force and torque sensing for serial manipulator based on an adaptive Kalman filter with variable time period. *Robotics and Computer-Integrated Manufacturing* 2021; 72: 102210. <https://doi.org/10.1016/j.rcim.2021.102210>
- [7] Ashwin KP, Mahapatra SK, Ghosal A. Profile and contact force estimation of cable-driven continuum robots in presence of obstacles. *Mechanism and Machine Theory* 2021; 64: 104404. <https://doi.org/10.1016/j.mechmachtheory.2021.104404>
- [8] Wang Z, Zi B, Wang D, Qian J, You W et al. External force self-sensing based on cable-tension disturbance observer for surgical robot end-effector. *IEEE Sensors Journal* 2019; 19 (13): 5274-5284. <https://doi.org/10.1109/JSEN.2019.2903776>
- [9] Liu X, Zhao F, Ge SS, Wu Y, Mei X. End-effector force estimation for flexible-joint robots with global friction approximation using neural networks. *IEEE Transactions on Industrial Informatics* 2019; 15 (3): 1730-1741. <https://doi.org/10.1109/TII.2018.2876724>
- [10] Peng G, Yang C, He W, Chen CLP. Force sensorless admittance control with neural learning for robots with actuator saturation. *IEEE Transactions on Industrial Electronics* 2020; 67 (4): 3138-3148. <https://doi.org/10.1109/TIE.2019.2912781>
- [11] Ren T, Dong Y, Wu D, Chen K. Collision detection and identification for robot manipulators based on extended state observer. *Control Engineering Practice* 2018; 79: 144-153. <https://doi.org/10.1016/j.conengprac.2018.07.004>
- [12] Han S, Wang H, Tian Y, Yu H. Enhanced extended state observer-based model-free force control for a series elastic actuator. *Mechanical Systems and Signal Processing* 2023; 183: 109584. <https://doi.org/10.1016/j.ymsp.2022.109584>
- [13] Murakami T, Nakamura R, Yu F, Ohnishi K. Force sensorless impedance control by disturbance observer. In: *Proceedings of the Power Conversion Conference*; Yokohama, Japan; 1993. pp. 352-357. <https://doi.org/10.1109/PCCON.1993.264158>
- [14] Katsura S, Irie K, Ohishi K. Wideband force control by position-acceleration integrated disturbance observer. *IEEE Transactions on Industrial Electronics* 2008; 55 (4): 1699-1706. <https://doi.org/10.1109/TIE.2007.907664>
- [15] Phuong T, Ohishi K, Yokokura Y. Fine sensorless force control realization based on dither periodic component elimination Kalman filter and wide band disturbance observer. *IEEE Transactions on Industrial Electronics* 2018; 67 (1): 757-767. <https://doi.org/10.1109/TIE.2018.2883256>
- [16] Samuel K, Oboe R, Oh S. A reduced-order multisensor-based force observer. *IEEE Transactions on Industrial Electronics* 2021; 69 (5): 4946-4956. <https://doi.org/10.1109/TIE.2021.3086719>
- [17] Park Y, Paine N, Oh S. Development of force observer in series elastic actuator for dynamic control. *IEEE Transactions on Industrial Electronics* 2017; 65 (3): 2398-2407. <https://doi.org/10.1109/TIE.2017.2745457>
- [18] Sariyildiz E, Ohnishi K. A comparison study for force sensor and reaction force observer based robust force control systems. In: *IEEE International Symposium on Industrial Electronics*; İstanbul, Türkiye; 2014. pp. 1156-1161. <https://doi.org/10.1109/ISIE.2014.6864777>
- [19] Sariyildiz E. A stability analysis for the reaction torque observer-based sensorless force control systems. In: *2023 IEEE International Conference on Mechatronics*; Loughborough, UK; 2023. pp. 1-5. <https://doi.org/10.1109/ICM54990.2023.10101940>

- [20] Sariyildiz E, Hangai S, Uzunovic T, Nozaki T. Discrete-time analysis and synthesis of disturbance observer-based robust force control systems. *IEEE Access* 2021; 9: 148911-148924. <https://doi.org/10.1109/ACCESS.2021.3123365>
- [21] Kurumatani H, Katsura S. Design of nominal parameters for robust sensorless force control based on disturbance observer. *IEEJ Journal of Industry Applications* 2019; 8 (2): 342-351. <https://doi.org/10.1541/ieejia.8.342>
- [22] Shimamoto K, Murakami T. Performance evaluation of force control and reaction force estimation in force sensorless hybrid control for workspace based controller. In: *IEEE 17th International Conference on Advanced Motion Control*; Padova, Italy; 2022. pp. 231-236. <https://doi.org/10.1109/AMC51637.2022.9729321>
- [23] Nagai S, Oboe R, Shimono T, Kawamura A. Fast force control without force sensor using combination of aaKF and RFOB for in-circuit test with probing system. *IEEJ Journal of Industry Applications* 2019; 8 (2): 152-159. <https://doi.org/10.1541/ieejia.8.152>
- [24] Nagai S, Kawamura A. Position/force sensorless force control using reaction force observer for compact dual solenoid actuator. In: *45th Annual Conference of the IEEE Industrial Electronics Society*; Lisbon, Portugal; 2019. pp. 3635-3640. <https://doi.org/10.1109/IECON.2019.8926848>
- [25] Azimi V, Nguyen T, Sharifi M, Fakoorian S, Simon D. Robust ground reaction force estimation and control of lower-limb prostheses: theory and simulation. *IEEE Transactions on Systems, Man, and Cybernetics: Systems* 2018; 50 (8): 3024-3035. <https://doi.org/10.1109/TSMC.2018.2836913>
- [26] Sariyildiz E, Ohnishi K. An adaptive reaction force observer design. *IEEE/ASME Transactions on Mechatronics* 2015; 20 (2): 750-760. <https://doi.org/10.1109/TMECH.2014.2321014>
- [27] Sariyildiz E, Oboe R, Ohnishi K. Disturbance observer-based robust control and its applications: 35th anniversary overview. *IEEE Transactions on Industrial Electronics* 2020; 67 (3): 2042-2053. <https://doi.org/10.1109/TIE.2019.2903752>
- [28] Sariyildiz E, Ohnishi K. On the explicit robust force control via disturbance observer. *IEEE Transactions on Industrial Electronics* 2014; 62 (3): 1581-1589. <https://doi.org/10.1109/TIE.2014.2361611>
- [29] Mitsantisuk C, Ohishi K, Katsura S. Variable mechanical stiffness control based on human stiffness estimation. In: *IEEE International Conference on Mechatronics*; İstanbul, Türkiye; 2011. pp. 731-736. <https://doi.org/10.1109/ICMECH.2011.5971211>
- [30] Baran EA, Uzunovic T, Sabanovic A. Performance improvement of bilateral control systems using derivative of force. *Robotica* 2018; 36 (11): 1613-1626. <https://doi.org/10.1017/S0263574718000607>